AAS 15-773

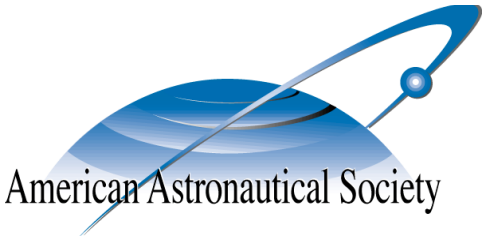

American Institute of
Aeronautics and Astronautics

CONTINUOUS-TIME MODELING AND CONTROL USING LINEARIZED RELATIVE ORBIT ELEMENTS

Trevor Bennett and Hanspeter Schaub

AAS/AIAA Astrodynamics Specialists Conference

Vail, CO **August 9–13 , 2015**

AAS Publications Office, P.O. Box 28130, San Diego, CA 92198

(Preprint) AAS 15-773

CONTINUOUS-TIME MODELING AND CONTROL USING LINEARIZED RELATIVE ORBIT ELEMENTS

Trevor Bennett* **and Hanspeter Schaub†**

Motivated by the breadth of applications for relative orbit control in formation flying and proximity operations, a new approach to the time-varying Clohessy-Wiltshire (CW) equations is developed. The Lagrangian Brackets variations enable study of invariants in the presence of perturbation accelerations. The Lagrangian Brackets are applied to the constants in the linear CW equations, called Linearized Relative Orbit Elements or LROEs, to provide equations of motion. The geometrical relative motion insights are investigated when drag perturbations are included. In addition, a LROE feedback control law to transition between relative orbits is developed and numerically assessed. The manuscript concludes with relative orbit reconfiguration optimization fundamentals and discussion of additional work.

INTRODUCTION

Relative orbit control has applications in satellite formations, rendezvous and docking, and sensing missions. The relative motion between two spacecraft can be described using a variety of parameterizations and assumptions. The breadth of relative motions descriptions share fundamental development approaches and assumptions and are grouped together under the title Relative Orbit Elements (ROEs). Desired, in all cases, is the motion of a deputy craft relative to the chief craft. The relative motion is obtained by a difference between the deputy and chief element sets. Often, linear assumptions and dynamic simplifications are utilized to reduce complexity and enable analytical solutions. A few researchers have explored the variations of the element sets to produce a applicable relative motion descriptions.[?] Several spacecraft missions are beginning to implement ROE control schemes particularly on small and CubeSat missions.[?,1,2] This manuscript classifies and sorts existing ROEs, develops equations of motion for a new branch of the ROE family, and provides the foundation for simplified ROE control approaches.

The ROEs can be organized in a tree structure with two major limbs: orbit element differences of the nonlinear inertial motion and orbit element differences of the linearized motion. The set of inertial motion orbit element differences encompasses the development of inertial vector differencing in obtaining relative orbit elements. One such common formulation is the differencing of classical orbit elements.[3–5] Orbit element differencing has also manifested itself in eccentricity and inclination vector separation descriptions.[6] As exhibited by the PRISMA mission, inertial differencing can remain in the Cartesian frame, especially when using Cartesian position provided by GPS.[7]

*Graduate Research Assistant, Aerospace Engineering Sciences, University of Colorado.
†Professor, Department of Aerospace Engineering Sciences, University of Colorado, 431 UCB, Colorado Center for Astrodynamics Research, Boulder, CO 80309-0431

Additional orbit element differences have been explored for control effectiveness.[8] In general, the inertial differencing provides greater fidelity often at the cost of computation.

The alternate limb of ROEs are elements of the linearized motion. Consider the well-know Clohessy-Wiltshire (CW) equations derived as the analytical solution of the linearized motion about a circular chief location.[9] The CW equations provide clear geometrical insight into spacecraft relative motion as a combination of ellipse scaling and phase angles with many Low-Earth Orbit (LEO) applications, CubeSat missions, and orbits near the Geostationary (GEO). The ROEs of the CW equations are first extensively explored by References 10 and 11. Defining orbit elements of the linearized motion prescribes the set of ROEs from the CW equations as Linearized ROEs or LROEs. The CW ROEs are applied to continuous thrust reconfiguration maneuvers in the past, however at the expense of requiring input shaping.[12] Further exploration has begun on curvilinear and nonlinear transformations of the linearized motion, however the formulations suffer from the same drawbacks of described LROE control formations.[13] The greater body of LROE formulations to-date is collected in Reference 14 with time-varying additions included.

This study presents further expansion of relative motion control by applying variational mathematics to long-standing analytical solutions to deliver simple feedback control methodologies. Motivated by the range of applicability, the 6 elements of the CW equations' unperturbed motion are further investigated. As described, these constants provide intuitive shaping of relative motion. These constants may be used as a relative orbit element set if the evolution of these parameters is developed in the presence of perturbation influences. This enables the inclusion of differential drag, coulomb formations, and other mission relevant perturbation forces studied by other authors.[15,16] The following sections implement variation mathematics to derive the time-evolving elements, apply established control methods using the new variation form, and expand upon the insight and applicability gained.

LINEARIZED RELATIVE ORBIT ELEMENTS (LROES)

The CW equations provide a convenient form for directly prescribing the relative orbit and are often utilized for geometric insight. The magnitudes of the scaling and phasing terms enable direct shaping of the relative orbit. It is the intuitive nature of these constants that motivates the following development. Recall the CW equation form as the analytical solution to the linearized relative motion shown in Eq. (1) with associated rates in Eq. (2).[17] The constants that appear in the CW equations are invariants of the unperturbed linearized motion. These invariants are considered as a set of relative orbit elements (ROEs). As this set of ROEs is derived from the linearized motion solution, the invariant vector of the CW equations is refered to as a Linearized ROE or LROE. The Hill frame position vector components are[17,18]

$$x(t) = A_0 \cos(nt + \alpha) + x_{\text{off}} \tag{1a}$$
$$y(t) = -2A_0 \sin(nt + \alpha) - 1.5ntx_{\text{off}} + y_{\text{off}} \tag{1b}$$
$$z(t) = B_0 \cos(nt + \beta) \tag{1c}$$

with the velocity vector expressed as

$$\dot{x}(t) = -A_0 n \sin(nt + \alpha) \tag{2a}$$
$$\dot{y}(t) = -2A_0 n \cos(nt + \alpha) - 1.5nx_{\text{off}} \tag{2b}$$
$$\dot{z}(t) = -B_0 n \sin(nt + \beta) \tag{2c}$$

Given the initial invariants of motion A_0, α, B_0, β, x_{off}, y_{off}, the CW equations provide a position and velocity of the deputy spacecraft about the reference orbit. The time derivative of the CW equations provides the relative motion rates in Eq. (2). Given both position and velocity measures, a typical relative state vector and set of LROEs are defined in Eq (3).

$$\boldsymbol{s} = \begin{bmatrix} x \\ y \\ z \\ \dot{x} \\ \dot{y} \\ \dot{z} \end{bmatrix} = \begin{bmatrix} \boldsymbol{r} \\ \boldsymbol{v} \end{bmatrix} \qquad \boldsymbol{e} = \begin{bmatrix} A_0 \\ \alpha \\ B_0 \\ \beta \\ x_{\text{off}} \\ y_{\text{off}} \end{bmatrix} \tag{3}$$

An inverse mapping between a typical state $\boldsymbol{s}$ and the LROEs is obtained in Eq. (4) where the current mean motion and time of the chief spacecraft are used.

$$A_0 = \frac{\sqrt{9n^2x^2 + \dot{x}^2 + 12nx\dot{y} + 4\dot{y}^2}}{n} \tag{4a}$$

$$\alpha = \tan^{-1}\left(\frac{\dot{x}}{-3nx - 2\dot{y}}\right) - nt \tag{4b}$$

$$B_0 = \frac{\sqrt{n^2z^2 + \dot{z}^2}}{n} \tag{4c}$$

$$\beta = \tan^{-1}\left(\frac{-\dot{z}}{nz}\right) - nt \tag{4d}$$

$$x_{\text{off}} = 4x + 2\frac{\dot{y}}{n} \tag{4e}$$

$$y_{\text{off}} = -2\frac{\dot{x}}{n} + y + (6nx + 3\dot{y})t \tag{4f}$$

The inverse mapping allows the relative motion parameters to be obtained at any point in time given the relative motion of the system as mapped from the CW Hill frame to LROE space. Consider the CW equations in Eq. (1) and the inverse mapping in Eq. (4). If the elliptical invariant A_0 or B_0 are zero in Eq. (1), then the angles α and β are ambiguous and lack influence. However, the inverse mapping introduces an inverse tangent function that is subject to singularities and the secular term nt that must be modulo 2π for consistency. This mapping is required unless additional logic is included or further reduced forms of the equations are used. The CW equations therefore are unable to provide a unique solution to the Leader-Follower configuration without modification. These singularities in the CW form motivate alternate or modified forms of the CW equations and invariant set.

NONSINGLUAR MODIFICATION TO THE LROE SET

Slight modification to the CW equations removes the α and β ambiguity and largely preserves the inherent insight. Proposed is a modified set of LROEs that utilizes the trigonometric expansions

$$A_0\cos(\alpha + nt) = A_0\cos(\alpha)\cos(nt) - A_0\sin(\alpha)\sin(nt)$$
$$A_0\sin(\alpha + nt) = A_0\sin(\alpha)\cos(nt) + A_0\cos(\alpha)\sin(nt)$$

where new constants A_1 and A_2 are defined.

$$A_1 = A_0 \cos(\alpha) \tag{6a}$$
$$A_2 = A_0 \sin(\alpha) \tag{6b}$$

The ambiguity of the linear combination of A_0 and α is removed in place of two perpendicular scaling terms. Additional definitions of the B_1 and B_2 invariants of the unperturbed relative motion are defined similarly to the A_1 and A_2. Using the simplifications in Eq (5) and Eq. (6), the CW solution is rewritten into the proposed LROE form

$$x(t) = A_1 \cos(nt) - A_2 \sin(nt) + x_{\text{off}} \tag{7a}$$
$$y(t) = -2A_1 \sin(nt) - 2A_2 \cos(nt) - 1.5ntx_{\text{off}} + y_{\text{off}} \tag{7b}$$
$$z(t) = B_1 \cos(nt) - B_2 \sin(nt) \tag{7c}$$

The time derivative of the CW equations provides the relative motion rates in Eq. (2).

$$\dot{x}(t) = -A_1 \sin(nt) - A_2 \cos(nt) \tag{8a}$$
$$\dot{y}(t) = -2A_1 n \cos(nt) + 2A_2 n \sin(nt) - 1.5nx_{\text{off}} \tag{8b}$$
$$\dot{z}(t) = -B_1 n \sin(nt) - B_2 \cos(nt) \tag{8c}$$

A new set of invariants are therefore defined. These invariants of the unperturbed motion are also LROEs, as they provide direct information regarding the geometry of the relative orbit from a linearized vector difference. The new LROE set is of all in units of distance providing additional simplicity.

$$\boldsymbol{e} = \begin{bmatrix} A_1 \\ A_2 \\ B_1 \\ B_2 \\ x_{\text{off}} \\ y_{\text{off}} \end{bmatrix} \text{ [m]} \tag{9}$$

The LROEs defined in Eq. (9) can be obtained at any point given Hill frame measurements or time history through an inverse mapping. The inverse mapping for the new LROE set is defined in Eq (10). The analytic inverse form allows Hill frame measurements to be easily mapped into LROE information.

$$A_1 = -\frac{(3nx + 2\dot{y})\cos(nt) + \dot{x}\sin(nt)}{n} \tag{10a}$$
$$A_2 = \frac{(3nx + 2\dot{y})\sin(nt) - \dot{x}\cos(nt)}{n} \tag{10b}$$
$$B_1 = z\cos(nt) - \frac{\dot{z}\sin(nt)}{n} \tag{10c}$$
$$B_2 = -z\sin(nt) - \frac{\dot{z}\cos(nt)}{n} \tag{10d}$$
$$x_{\text{off}} = 4x + \frac{2\dot{y}}{n} \tag{10e}$$
$$y_{\text{off}} = -\frac{2\dot{x}}{n} + y + (6nx + 3\dot{y})t \tag{10f}$$

LROEs both in the traditional and nonsingular forms provide the relative motion geometry in the absence of perturbation. Desired is the evolution of the elements when perturbations are present. The following section derives the Lagrangian Bracket formulation used to generate the specific LROE evolution equations.

LAGRANGIAN BRACKETS DEVELOPMENT OF LROE VARIATIONAL EQUATIONS

Of interest is the effect on the relative motion from either controlled or uncontrolled perturbations. Currently, the LROEs proposed are constants of motion. However, implementation of the Lagrangian Bracket formulation to the CW equations allows perturbation accelerations to influence the LROE values. The Lagrangian Bracket form evolves the relative motion elements when perturbed from Keplerian orbits. The Lagrangian Bracket form, detailed in Reference 17, evolves the invariants of motion present in a dynamical system's analytical solution to match the nonlinear solution at the prescribed time. Given the inverse mappings provided in Eq (4) and Eq (10), the sensitivity matrices are computable. The invariant vector $\boldsymbol{e}$, otherwise invariant, evolves according to Eq. (11) where $\boldsymbol{r}$ is the position vector and $\boldsymbol{a}_d$ is the disturbance acceleration.

$$\dot{\boldsymbol{e}} = [L]^{-1} \left[\frac{\partial \boldsymbol{r}}{\partial \boldsymbol{e}}\right]^T \boldsymbol{a}_d \tag{11}$$

where the Lagrangian Bracket matrix $[L]$ is defined by

$$[L] = \frac{\partial \boldsymbol{s}}{\partial \boldsymbol{e}}^T [J] \frac{\partial \boldsymbol{s}}{\partial \boldsymbol{e}} \tag{12}$$

and $[J]$ is the symplectic matrix of necessary dimension. A full development of the Lagrangian Bracket form is included in Reference 17.

The evolution of the invariants described by Eq. (11) enables an analytic solution to evolve to a non-homogeneous disturbance acceleration. The analytical solution for the relative orbit described by the CW equations is used where the considered state and invariants used in Eq. (11) are presented in Eq. (3). The partials necessary for Eq. (12) are developed by first defining the simplifying terms

$$\kappa_\alpha = nt + \alpha \qquad \kappa_\beta = nt + \beta \tag{13}$$

Completing the derivation of required matrices in Eq. (11), the partial derivatives of the relative position vector with respect to the invariants is presented in Eq. (14). The result in Eq. (14) constitutes the upper half of the the state-partials matrix where the remaining terms are left to the reader.

$$\frac{\partial \boldsymbol{r}}{\partial \boldsymbol{e}} = \begin{bmatrix} \cos(\kappa_\alpha) & -A_0 \sin(\kappa_\alpha) & 0 & 0 & 1 & 0 \\ -2\sin(\kappa_\alpha) & -2A_0 \cos(\kappa_\alpha) & 0 & 0 & -1.5nt & 1 \\ 0 & 0 & \cos(\kappa_\beta) & -B_0 \sin(\kappa_\beta) & 0 & 0 \end{bmatrix} \tag{14}$$

Introducing the derived partials into Eq. (12) and simplifying yields the full Lagrangian Bracket form and inverse in Eq. (15). The sparsely populated matrices are presented in component form

where the skew symmetric property is required to build the full matrices.

$$
\begin{aligned}
L_{1,2} &= -5A_0 n & L_{1,2}^{-1} &= -3/(A_0 n) \\
L_{1,5} &= -3n^2 t\cos(\kappa_\alpha) + 4n\sin(\kappa_\alpha) & L_{1,5}^{-1} &= -4\sin(\kappa_\alpha)/n \\
L_{1,6} &= 2n\cos(\kappa_\alpha) & L_{1,6}^{-1} &= -8\cos(\kappa_\alpha)/n - 6t\sin(\kappa_\alpha) \\
L_{2,5} &= A_0 n(4\cos(\kappa_\alpha) + 3nt\sin(\kappa_\alpha)) & L_{2,5}^{-1} &= -4\cos(\kappa_\alpha)/(A_0 n) \\
L_{2,6} &= -2A_0 n\sin(\kappa_\alpha) & L_{2,6}^{-1} &= (8\cos(\kappa_\alpha) - 6nt\sin(\kappa_\alpha))/(A_0 n) \\
L_{3,4} &= -B_0 n & L_{3,4}^{-1} &= 1/(B_0 n) \\
L_{5,6} &= 3/2n & L_{5,6}^{-1} &= 10/n
\end{aligned}
\tag{15}
$$

The classical element form is therefore fully defined. The following section addresses the modified LROE set.

MODIFIED LROE LAGRANGIAN BRACKETS DEVELOPMENT

The substitution made in Eq. (7) removes the ambiguity in defining α and β for configurations where the scaling element is zero. Following the same approach used to develop the Lagrangian Brackets for the classical CW form, this section develops the Lagrangian Brackets for the modified LROEs. Taking the partials of the CW state with respect to the LROEs provides the necessary state-partials matrix with the position partials shown.

$$
\frac{\partial \boldsymbol{s}}{\partial \boldsymbol{e}} = \begin{bmatrix} \cos(nt) & \sin(nt) & 0 & 0 & 1 & 0 \\ -2\sin(nt) & -2\cos(nt) & 0 & 0 & -3/2nt & 1 \\ 0 & 0 & \cos(nt) & -\sin(nt) & 0 & 0 \end{bmatrix} \tag{16}
$$

Carrying out the symplectic matrix operation in Eq. 12 generates the modified LROE Lagrangian Brackets and inverse. Again, the sparsely populated matrices, in Eq. (17), are presented in component form noting the final matrices is also skew symmetric.

$$
\begin{aligned}
L_{1,2} &= -5n & L_{1,2}^{-1} &= -3/n \\
L_{1,5} &= -3n^2 t\cos(nt) + 4n\sin(nt) & L_{1,5}^{-1} &= -4\sin(nt)/n \\
L_{1,6} &= 2n\cos(nt) & L_{1,6}^{-1} &= -8\cos(nt)/n - 6t\sin(nt) \\
L_{2,5} &= 4n\cos(nt) + 3n^2 t\sin(nt) & L_{2,5}^{-1} &= -4\cos(nt)/n \\
L_{2,6} &= -2n\sin(nt) & L_{2,6}^{-1} &= 8\cos(nt)/n - 6t\sin(nt) \\
L_{3,4} &= -n & L_{3,4}^{-1} &= 1/n \\
L_{5,6} &= 3/2n & L_{5,6}^{-1} &= 10/n
\end{aligned}
\tag{17}
$$

Apparent in Eq 17 is that only the mean motion appears in the denominator of the inverse. Removal of the scaling terms from the denominator in the Lagrangian Brackets removes the singularities present in Eq. (15). The non-singular form using the modified LROEs is carried forward for the remainder of this study. It can also be shown that the Poisson Brackets approach confirms the Lagrangian Brackets forms presented.

PERTURBATION EFFECTS PRESENT IN MODIFIED LROES

Inclusion of perturbation effects in the relative motion are apparent and intuitive when represented in LROE space. A dominant perturbation for spacecraft in LEO is atmospheric drag. Consider the influence of drag on a spacecraft defined by the drag acceleration model in Eq. (18).

$$\ddot{\boldsymbol{r}} = -\frac{1}{2} C_D \frac{A}{m} \rho_A \|\boldsymbol{V}_A\| \boldsymbol{V}_A \tag{18}$$

The drag model constants and variables in Equation 18 utilized by this study assume equivalent spacecraft defined by

$$\begin{aligned} A &= 3.0\ [m^2] \\ m &= 970\ [kg] \\ \rho_0 &= 3.614 \times 10^{-13}\ [kg/m^3] \\ r_0 &= (700000.0 + R_{Earth})\ [m] \\ H &= 88667.0\ [m] \\ \rho_A &= \rho_0 \exp -(r - r_0)/H \\ \boldsymbol{V}_A &= \begin{bmatrix} \dot{r_X} + \dot{\theta} r_Y \\ \dot{r_Y} - \dot{\theta} r_X \\ \dot{r_Z} \end{bmatrix} \end{aligned}$$

where ρ_0 is a reference atmospheric density, r_0 is a reference radius, H is a scaling height, and $\boldsymbol{r}$ is the position of the spacecraft. The contribution from rotation of the Earth's atmosphere includes the Earth spin rate in Equation 19 where t is the time in seconds past the epoch.

$$\theta = t \cdot 7.2921158553 \times 10^{-5}\ [\text{rad}] \tag{19}$$

Consider the influence of the described drag model during maintenance of a planar ellipse spacecraft formation defined by the reference LROE set

$$\boldsymbol{e}_r = \begin{bmatrix} A_{1,r} \\ A_{2,r} \\ B_{1,r} \\ B_{2,r} \\ x_{\text{off},r} \\ y_{\text{off},r} \end{bmatrix} = \begin{bmatrix} 20 \\ 0 \\ 0 \\ 0 \\ 0 \\ 0 \end{bmatrix}\ [\text{m}]$$

Drag is applied to each spacecraft in the numerical analysis initialized an equatorial circular LEO chief with a semi-major axis of $a = 7550$ km. The simulated inertial state is composed of position and velocity for both uncontrolled chief spacecraft and controlled deputy spacecraft. The simulations are propagated for a duration of 10 chief orbits at $\Delta t = 0.5$ seconds and drag as the only non-Keplerian perturbation. The difference between actual and desired relative orbit is shown in Figure 1.

Figure 1 reflects the effect of drag on relative orbit geometry. The LROE parameters shown are extracted at each time step using the inverse mapping provided. The out-of-plane B_1 and B_2

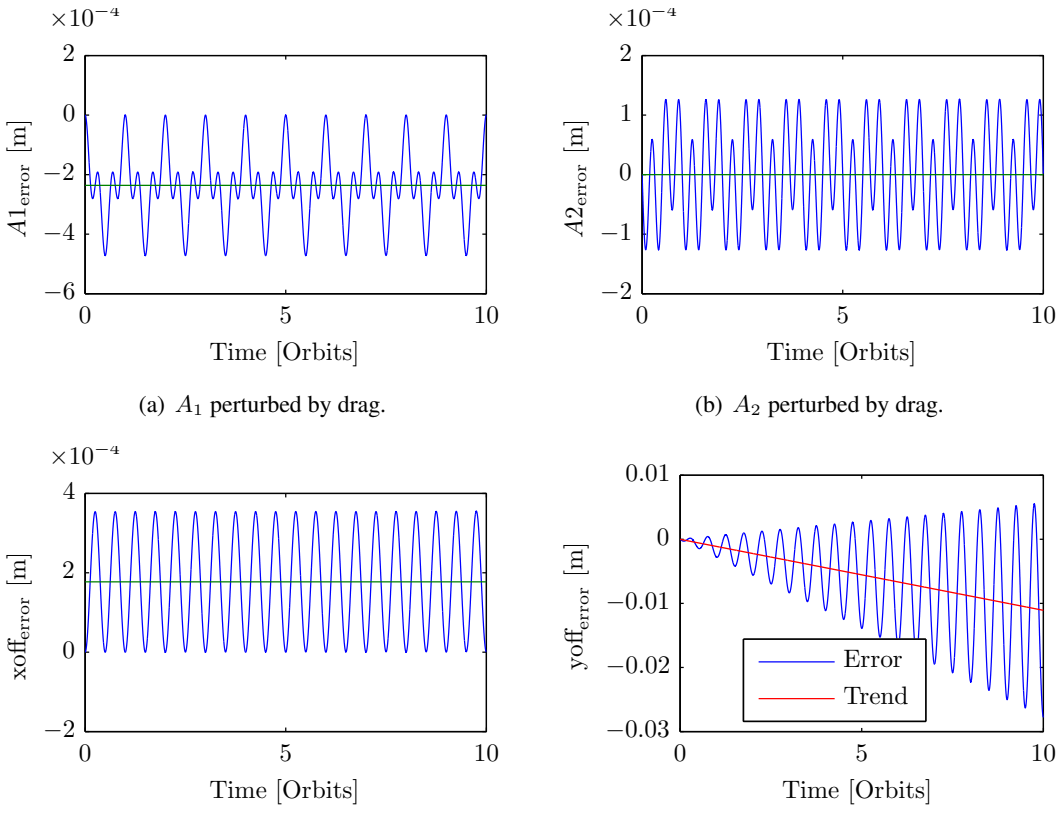

(a) A_1 perturbed by drag.

(b) A_2 perturbed by drag.

(c) x_{off} perturbed by drag.

(d) y_{off} perturbed by drag.

Figure 1. LROE error from unperturbed in the presence of drag. Mean shown in .

parameters remain zero and are not shown. Most notable are the x_{off} error in Figure 1(c) and the y_{off} error in Figure 1(d). The mean x_{off} is a non-zero constant. As expected, this shears the relative motion apart witht the y_{off} trend linearly diverging from a bounded formation. The A_2 component in Figure 1(b) maintains a zero mean as expected. The geometry of the ellipse in the along-track direction, as captured by the A_2 parameter, remains unchanged while the y_{off} grows. The A_1 parameter however exhibits a non-zero constant error.

On-going investigation uses the Lagrange Bracket relation in Eq. (11) to predict the LROE variations using perturbation effect models in the relative frame. Predictive LROE models enable relative navigation with more realistic extensive propagation. In addition, the relative motion control is able to account for perturbation effects. The usefulness of LROE variational equations enables both perturbation modelling as well as injecting a desired acceleration. The following section develops a control scheme that injects an accleration to maintain or reconfigure a relative orbit.

LAGRANGIAN BRACKETS CONTROL DEVELOPMENT

Utilization of the input acceleration in the Lagrange Bracket form, a control law that drives the relative motion of two satellites to a desired geometry is developed. The LROE vector $\boldsymbol{e}$, otherwise invariant, evolves according to Eq. (11) where $\boldsymbol{r}$ is the position vector in $\boldsymbol{s}$ and $\boldsymbol{a}_d$ is the disturbance acceleration. Leveraging Eq. (11), a desired reference evolution of the geometrical parameters in $\boldsymbol{e}$

can be implemented to transition from one relative orbit to another. The equations of motion for the LROEs is defined for the control development by the simplification

$$\dot{\boldsymbol{e}} = [B]\boldsymbol{u} \qquad \text{where} \qquad [B] = [L]^{-1}\left[\frac{\partial \boldsymbol{r}}{\partial \boldsymbol{e}}\right]^T \tag{20}$$

The form of Eq. (20) demonstrates the expected type of response to proper control influence. Noting that the disturbance acceleration $\boldsymbol{a}_d$ is included in the control law, feed forward of disturbance forces should be possible. The matrix $[B]$ for both classical and modified LROE sets are included in Eq. 21 and Eq. (22) respectively.

$$[B]_{\text{classic}} = \frac{1}{n}\begin{bmatrix} -\sin(\alpha+nt) & -2\cos(\alpha+nt) & 0 \\ -\cos(\alpha+nt)\frac{1}{A_0} & 2\sin(\alpha+nt)\frac{1}{A_0} & 0 \\ 0 & 0 & -\sin(\beta+nt) \\ 0 & 0 & -\cos(\beta+nt)\frac{1}{B_0} \\ 0 & 2 & 0 \\ -2 & 3nt & 0 \end{bmatrix} \tag{21}$$

$$[B]_{\text{modified}} = \frac{1}{n}\begin{bmatrix} -\sin(nt) & -2\cos(nt) & 0 \\ -\cos(nt) & 2\sin(nt) & 0 \\ 0 & 0 & -\sin(nt) \\ 0 & 0 & -\cos(nt) \\ 0 & 2 & 0 \\ -2 & 3nt & 0 \end{bmatrix} \tag{22}$$

Eq. 22 demonstrates further the advantage of the nonsingular formulation where the scaling terms do not appear in the denominator. This equation of motion enables the use of Lyapunov stability analysis to derive a suitable control law. The LROE error measure is therefore defined.

$$\Delta\boldsymbol{e} = \boldsymbol{e} - \boldsymbol{e}_r \tag{23a}$$

$$\Delta\dot{\boldsymbol{e}} = \dot{\boldsymbol{e}} - \dot{\boldsymbol{e}}_r = [B](\boldsymbol{u} - \boldsymbol{u}_r) \tag{23b}$$

The time rate of the LROE error measure also allows the reference trajectory to be defined by a LROE rate. While this capability is not yet studied, applications include prescribed relative orbit evolution, direct circumnavigation reference trajectories, and faster than natural circumnavigation.

Psuedo-Inverse Control Methodology

Employed is Lyapunov's direct method for obtaining a suitable control law to drive the LROEs to reference values. The approach utilized in Reference 17 does not provide a complete stability for a pseudo-inverse control law. However, the psuedo-inverse control is enticing due to the 6×6 gain matrix allowing element-specific tuning. Consider the newly proposed Lyapunov function defined in Eq. (24) where $[K]$ is a symmetric positive definite gain matrix.

$$V(\Delta\boldsymbol{e}) = \frac{1}{2}\Delta\boldsymbol{e}^T[K]\Delta\boldsymbol{e} \tag{24}$$

The time derivative of the Lyapunov function is

$$\dot{V}(\Delta\boldsymbol{e}) = \Delta\boldsymbol{e}^T[K]\Delta\dot{\boldsymbol{e}} \tag{25}$$

Inserting the error rate definition of Eq. (23) into Eq. (25) is shown in Eq. (26) equated to the desired Lyapunov derivative form. Without loss of generality, the control vector $\boldsymbol{u}$ is assumed to include the reference control $\boldsymbol{u}_r$. The desired symmetric negative-definite form is obtained with the symmetric positive-definite matrix $[P]$.

$$\dot{V}(\Delta \boldsymbol{e}) = \Delta \boldsymbol{e}^T [K][B]\boldsymbol{u} \quad \Rightarrow \quad -\boldsymbol{y}^T [P]\boldsymbol{y} \tag{26}$$

The following control law is proposed

$$\boldsymbol{u} = -([B]^T[B])^{-1}[B]^T[K]\Delta \boldsymbol{e} \tag{27}$$

To prove stability, the following definitions are made. The sub-element $([B]^T[B])^{-1}$ is a symmetric positive definite 3×3 matrix. The additional terms are collected into the vector $\boldsymbol{y}$.

$$[P] = ([B]^T[B])^{-1} \tag{28a}$$

$$\boldsymbol{y} = [B]^T[K]\Delta \boldsymbol{e} \tag{28b}$$

The desired Lyapunov time derivative defined in Eq. (26) is only a negative semi-definite form which guarantees only Lyapunov stability. For desired asymptotic stability, the sub-element of the Lyapunov time derivative $\boldsymbol{y}$ must be zero only when the LROE error is zero. Since the matrix $[K]$ is chosen to be positive definite, the term $[K]\Delta \boldsymbol{e}$ is always non-zero if the error is zero. However, due to the time variation of the B matrix, there are instantaneous points in time where $\boldsymbol{y}$ is zero. Although the combination of $[B]^T[K]\Delta \boldsymbol{e}$ may instantaneously go to zero, the largest invariant set where the product remains zero for all time is where $\Delta \boldsymbol{e}$ is zero at which point the control effort is zero. Thus LaSalle's Invariant principle delivers asymptotic stability.

The gains in the positive definite matrix $[K]$ for the proposed control are selected via three steps. First, expanding the $([B]^T[B])^{-1}[B]^T[K]$ product, some terms appear as $1/t$ or $1/t^2$. The gain terms preceding these higher order terms are set to zero for simplicity because the influence depletes as time moves towards infinity. This process eliminates most of the off-diagonal terms. It is therefore reasonable to assume a diagonal form for $[K]$ for the remainder of this study. Second, for a formation to be bounded or constrained to the desired drift the x_{off} term must be as exact as possible. Thus, the gain for this term is set to an order of magnitude larger than the other errors in the LROE feedback. Third, the inverse LROE mapping in Eq. (10) is sensitive to large accelerations that switch the sign of the velocity too quickly. Inserting a mean motion multiplicative factor serves to spread the error over an entire orbit. Inspection of Eq. (10) as well as numerical simulations demonstrate that large shifts and significantly large gains cause an instantaneous shift in the LROEs obtained by the inverse mapping. Such rapid shift introduce error measures orders of magnitude larger leading to divergence. The gain developed for the LROE controller in this study is set to:

$$[K] = n \cdot \text{diag}([1,\ 1,\ 1,\ 1,\ 30,\ 1]) \tag{29}$$

The gain matrix utilized may not be optimal, however sufficient performance is obtained. Future studies will address the gain matrix and seek dynamical system leverage in scaling the gain values. The LROE feedback controller is fully developed and defined. The Psuedo-Inverse method developed is implemented in several relative orbit reconfigurations detailed in the following sections.

Alternate Control Forms

The LROE form shares many similarities to the control implementation for orbit element differences. Recall that the prescribed error form is a relative orbit element difference of the linearized motion. Capitalizing on the parallels with orbit element differences, many other control forms available from orbit element difference control literature with a few shown in Reference 17. Additional forms may be possible, although the $[B]$ matrix defined by the current set of LROEs leads to a zero determinant for forms that include $[B][B]^T$ elements. The Psuedo-Inverse method derived in this study benefits more than other forms through use of a full 6×6 gain matrix that provides better element-specific tuning.

INERTIAL SIMULATION CONTROL IMPLEMENTATION

The proposed relative orbit description and associated control law are assessed using an inertial orbit simulation solving the full nonlinear 2-body problem. The numerical analysis assumes Keplerian orbits with a equitorial circular LEO chief with a semi-major axis of $a = 7550$ km. The simulated inertial state is composed of position and velocity for both uncontrolled chief spacecraft and controlled deputy spacecraft. The simulations are propagated for a duration of 10 chief orbits to fully illustrate the near steady state behavior. Three LROE reconfigurations are considered: from a planar ellipse to a lead-follower, from a lead-follower to the planar ellipse, and from a planar ellipse to a circularly projected relative orbit. The three cases demonstrate the breadth of controller ability and target specific singularities or coupling effects that render the classical CW parameterization insufficient. Presented are the initial and final desired LROE states. Notice that no time varying reference trajectory is prescribed for the transfer as the Lagrangian Brackets evolution provides the natural evolution given the current LROE error. Small relative orbits are considered for this study with two planar reconfiguration cases are produced. Both cases utilize full inertial non-linear simulation at an integration time step of 0.5 seconds.

Planar-Elliptic to Lead-Follower

The first case considered is the planar elliptic to the lead-follower. Desired is a transition from a zero offset 2-1 ellipse to a standoff distance in the along track direction ahead of the chief. The initial and final LROEs for this reconfiguration case are:

$$\boldsymbol{e}_0 = \begin{bmatrix} A_{1,0} \\ A_{2,0} \\ B_{1,0} \\ B_{2,0} \\ x_{\text{off},0} \\ y_{\text{off},0} \end{bmatrix} = \begin{bmatrix} 20 \\ 0 \\ 0 \\ 0 \\ 0 \\ 0 \end{bmatrix} \text{[m]} \qquad \boldsymbol{e}_r = \begin{bmatrix} 0 \\ 0 \\ 0 \\ 0 \\ 0 \\ 30 \end{bmatrix} \text{[m]}$$

The transfer between the initial and reference LROEs is achieved in greatest extent within 3 orbits of the chief. The Hill frame reconfiguration is shown in Figure 2 where the green signifies the initial relative orbit position and the magenta signifies the target lead-follower stand-off position. As can be seen in the Hill frame, the deputy satellite initial moves along a 2-1 ellipse as the along-track offset is increased. Over the following orbits, the ellipse shifts with slight expansion before contracting onto the reference point. By inspection, the size of the relative motion ellipse initially grows prescribed by the coupling in the variational equations in the along track position.

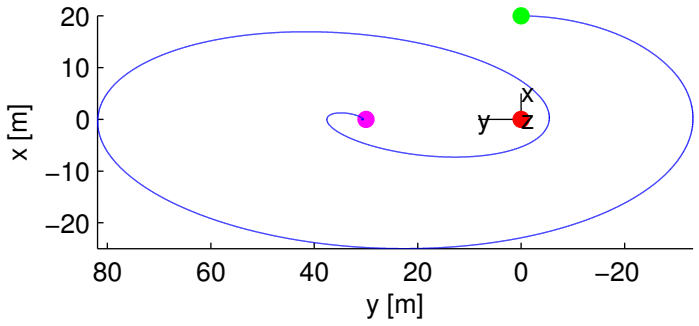

Figure 2. Hill frame convergence to Lead-Follower configuration.

The planar elliptic to lead-follower is a planar reconfiguration and therefore the de-coupled out-of-plane motion remains zero. The modified LROEs time history provides additional insight into the reconfiguration. Shown in Figure 3 are the time histories of the two scaling terms A_1 and A_2 as well as the along track and radial offsets. The simultaneous reconfiguration of the terms A_1 and y_{off} provide and interesting balance in the evolution of the relative orbit. Noteably, the first half orbit brings the x_{off} down and therefore the error up to sheer the deputy forward to the desired offset. The lightly damped but magnitude restricted response in x_{off} is due to the large gain placed on Δx_{off}. The current selection of a Δx_{off} error gain 30 times greater in magnitude than the other errors provides sufficient control authority without exceeding ± 2 meters of offset.Additional tuning of the x_{off} term may provide a range of performance with the limits of divergence if the gain is zero and no control authority if the gain is infinite. The combination of the scaling terms provides a noticeable effect in the Hill farme representation. Referring back to Figure 2, the relative ellipse appears to rotate. This effect is attributed to the collective variation in A_1 and A_2 after the transition in offset.

A logarithmic study of the LROE error shows the convergence behavior of the implemented control. Around the completion of 3 orbits, the controller is considered within sufficient accuracy of the reference location with additional convergence occurring over the following orbits. The logarithmic error for the LROEs is shown in Figure 4. As claimed, the majority of the error is reduced after completion of 3 orbits. The humped variation in the A_1 and A_2 parameters corresponds directly to the half orbit period. This error hump effect is due to the sine and cosine functions in the inverse mapping of Eq (10). As the point moves through a true zero for either sine or cosine, the resulting scaling term decreases towards zero. The offset terms, once the scaling term error has been removed, tend as a sustained decrease in error towards the simulation. The errors presented in Figure 4 are not expected to go to zero. The LROE formulation is a first order mapping with some error incurred by the inverse mapping. Thus the error obtained is near the best possible given the formulation and mapping equations. The chatter seen supports use of a dead-band control. It is believed that using a dead-band will prevent inverse mapping errors driving control acceleration once it is nearly converged.

The Hill frame control effort to produce the desired reconfiguration is shown in Figure 5. The top plot shows the first half of the reconfiguration where the bottom plot shows the logarithmic control effort. As can be seen in Figure 5, the primary control effort is in the intial radial direction, $\hat{\boldsymbol{X}}$. This is expected because the y_{off} is controlled through the drift incurred by an x_{off} and the A_1 scaling term is most dramatically reduced by the Hill x-direction acceleration. The slight y-direction

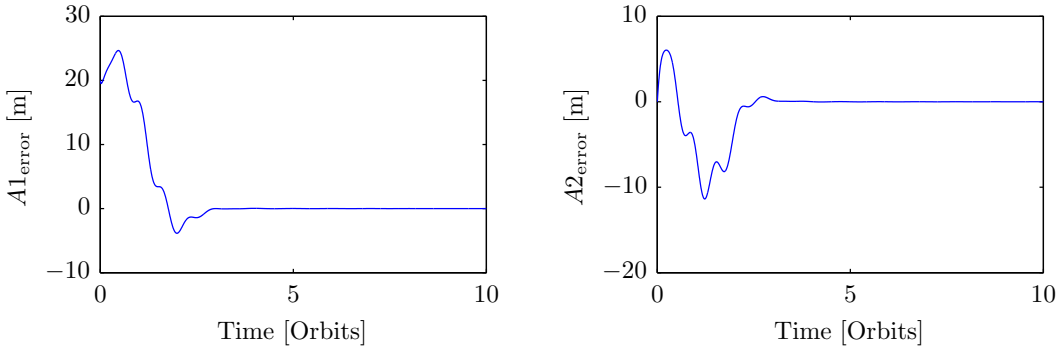

(a) A_1 Parameter Error

(b) A_2 Parameter Error

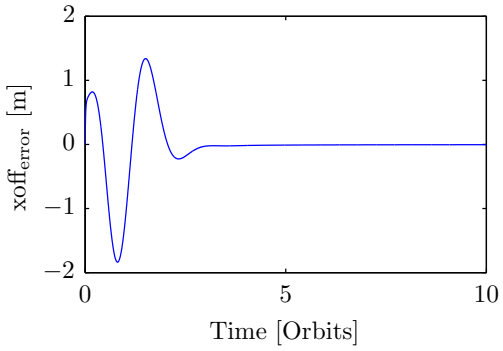

(c) x_{off} Parameter Error

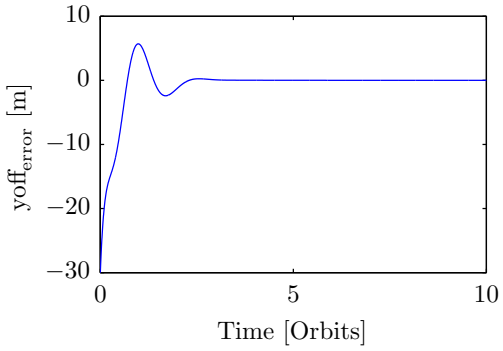

(d) y_{off} Parameter Error

Figure 3. LROE error for planar ellipse to lead-follower.

acceleration is present with the direct impact requiring further study. The logarithmic control effort suggests that the reconfiguration is primarily complete following the completion of the third orbit. The control gains assume a constant value that may be in part to the linearization error present in the LROE error formulation. The dramatic decrease does provide confidence that the controller does provide converged behavior.

The LROE control approach successfully reconfigures the relative orbit from a planar elliptic relative orbit to a lead-follower configuration. Otherwise infeasible with the classic CW form, the modified LROE form provides no singularities in the transfer space. A different control effort may be achieved if the initial position was described by a LROE of $A_2 \neq 0$. Further, some greater Hill y-direction thrusting might be present. This concept is explored in greater detail in the optimal transfer section and will be largely addressed by future work.

Lead-Follower to Planar-Elliptic

The second case considered is the lead-follower to the planar elliptic. Desired is the transition from a $y_{\text{off}} \neq 0$ to a 2-1 ellipse providing the inverse transfer of the first case. The initial and final LROEs for this reconfiguration case are:

$$\boldsymbol{e}_0 = \begin{bmatrix} 0 & 0 & 0 & 0 & 0 & 30 \end{bmatrix}^T \text{ [m]} \qquad \boldsymbol{e}_r = \begin{bmatrix} 20 & 0 & 0 & 0 & 0 & 0 \end{bmatrix}^T \text{ [m]}$$

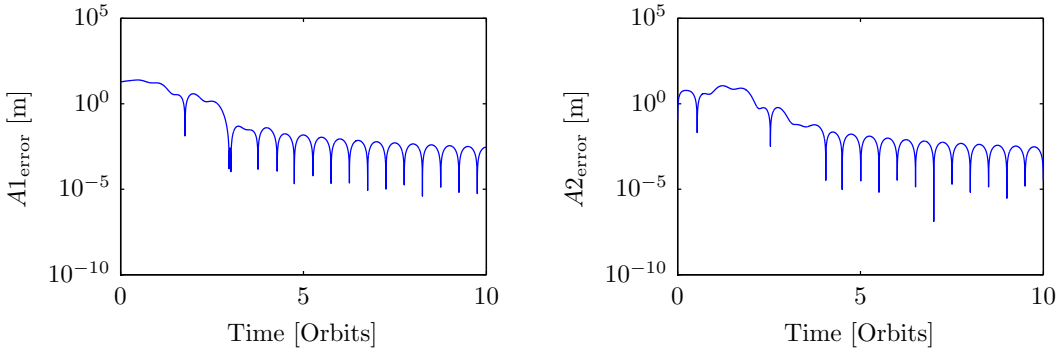

(a) A_1 Parameter Log Error

(b) A_2 Parameter Log Error

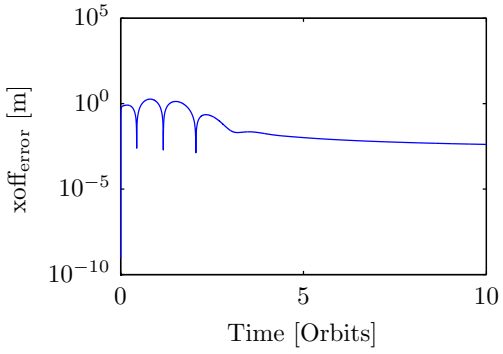

(c) x_{off} Parameter Log Error

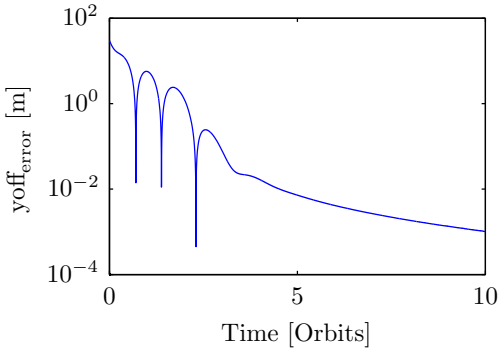

(d) y_{off} Parameter Log Error

Figure 4. Logarithmic LROE error for planar ellipse to lead-follower.

The transfer between the initial and reference LROEs is achieve in greatest extent within 3 orbits of the chief. The Hill frame reconfiguration is shown in Figure 6 where the green signifies the initial standoff position and the magenta signifies the target end position on the prescribed 2-1 ellipse. As can be seen in Figure 6, the deputy initially shifts the along track offset back towards the desired zero offset as the relative orbit scaling term is driven to a slightly decreased value. Once the controller moves the along-track error into the vicinity of zero, the controller drives the scaling term towards the increased value required for the 2-1 relative ellipse. The darker blue layered 2-1 ellipse demonstrates that following the third orbit, the deputy does remain on the prescribed 2-1 ellipse. The LROE errors for the lead-follower to planar elliptic case are presented in Figure 7.

Similar to the previous reconfiguration, the lead-follower to planar elliptic case shows a majority of the convergence within the first 3 orbits. As can be seen by Figure 7(a) and Figure 7(b), the first orbit is consumed by the y_{off} correction so the error grows. The A_1 error then decreases rapidly as the size of the ellipse expands. However, the error in the A_2 scaling term is present due to the inverse mapping coupling with the final corrections to the y_{off}. As in the previous case, the magnitude of the radial offset is restricted by the high gain value place on Δx_{off}.

The greatest insight gained from the LROE errors in Figure 7 are that the evolution is the negative of the evolution in the planar elliptic to lead-follower shown in Figure 3. A strongly supported conclusion is that the trajectory between two relative orbits follows the same evolution of LROEs

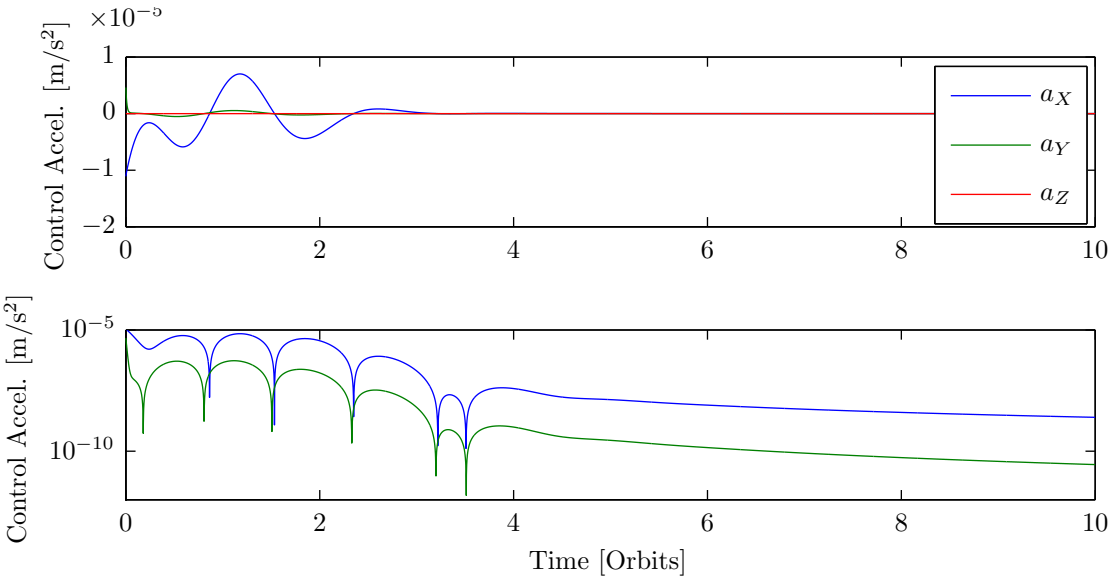

Figure 5. Hill frame deputy control effort from planar elliptic to lead-follower.

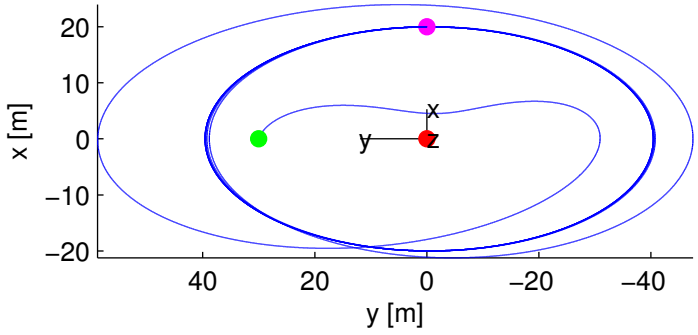

Figure 6. Hill frame convergence to planar ellipse configuration.

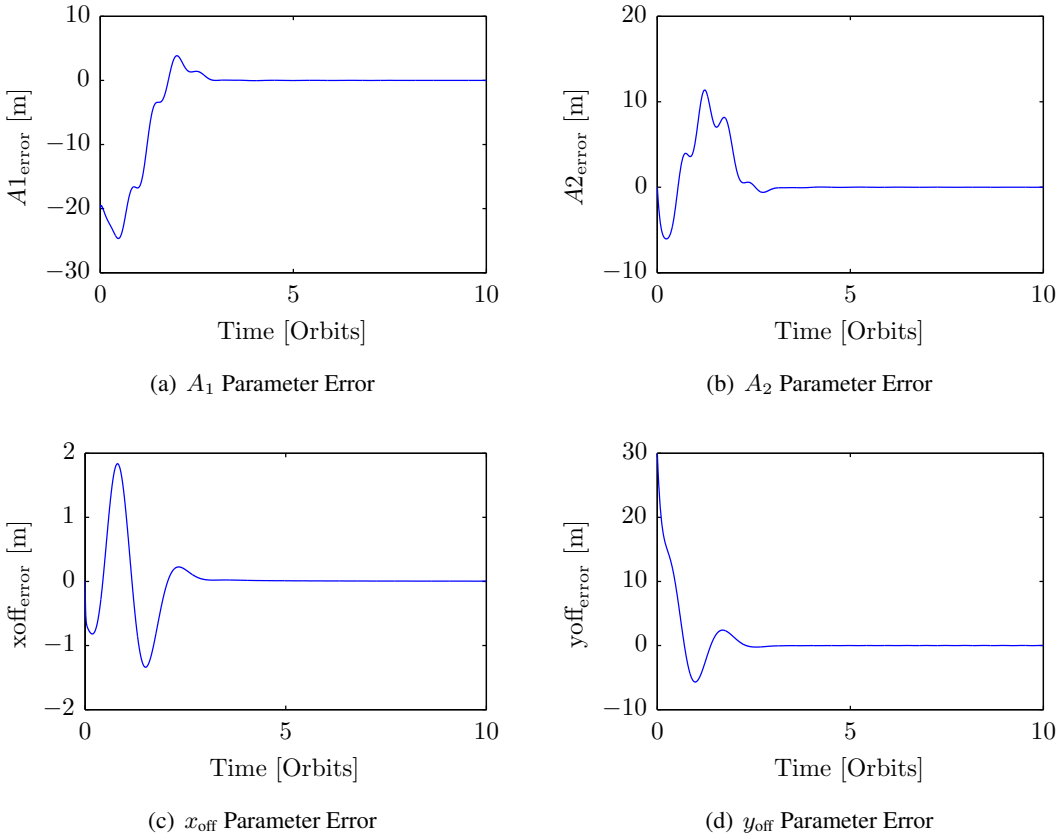

(a) A_1 Parameter Error

(b) A_2 Parameter Error

(c) x_{off} Parameter Error

(d) y_{off} Parameter Error

Figure 7. LROE error for lead-follower to planar ellipse.

in both the forward and reverse reconfiguration. Such consistent evolution between two relative orbits is inherent in the Lagrange Bracket formulation. This method then suggests that optimal reconfigurations may be obtained as a parameter sweep. This is addressed further in the optimization discussion in a later section.

Impressively, the LROE feedback controller generates suitable trajectories between the lead-follower and planar elliptic orbits. Analysis of both Figure 6 and Figure 2 reveal that the along-track offset is first corrected before the ellipse scaling factor A_1. Further analysis of the Lagrangian Brackets should reveal a greater sensitivity to the along-track position and the radial offset influence than the elliptic scaling factors.

OPTIMAL TRANSITIONS BETWEEN RELATIVE ORBITS

Given the analysis presented in this study, the continuous control provides a unique control law that leverages Lagrangian Brackets invariant evolution and the insight of LROE sets to develop the trajectory. In comparison, using a cartesian control law, which requires a reference trajectory to be defined, may not leverage the same dynamics benefit inherent in the LROE method. Capitalizing on this inherent use of dynamics the question of optimal transfers follows. Desired is an understanding of optimal reconfigurations using the 6 initial LROEs and the desired final LROE set. Returning to the observation that the evolution from elliptic to lead-follower and lead-follower to elliptic LROE

evolutions only differ by a sign, optimal transfers between orbit types may be resolved through parameter sweeps as the forward and reverse transfer are identical. That is, selecting an alternate initial time on the same initial orbit to define the initial LROEs may provide a more fuel optimal control.

The Lagrangian Brackets evolution provides the natural evolution given the current LROE error and therefore constitutes the open loop control implementation.Therefore, the objective of creating a open-loop control is demonstrated by the simple Lagrangian Bracket form. In the context of optimal reconfigurations a sampling of open loop trajectories, or more specifically an analysis of the Lagrangian Bracket form, may reveal desired open loop reconfigurations that are better. Initial investigation reveals the opportunity and availability of optimal reconfiguration in LROE space. Following is an initial example of optimal reconfiguration as applied to a deputy in a relative planar ellipse reconfiguring to a circularly projected relative orbit.

Planar-Elliptic to Circularly-Projected

The out-of-plane LROEs are now considered whereby an initial error in the scaling term B_1 is introduced. The initial and reference LROE sets for the nominal case are

$$\boldsymbol{e}_0 = \begin{bmatrix} 20 & 0 & 0 & 0 & 0 & 0 \end{bmatrix}^T \text{ [m]} \qquad \boldsymbol{e}_r = \begin{bmatrix} 20 & 0 & 40 & 0 & 0 & 0 \end{bmatrix}^T \text{ [m]}$$

The Hill frame position evolution with the implemented control is shown in Figure 8(a) with the initial point shown in green and the LROE prescribed position at the end of simulation shown in magenta. The relative orbit completes the primary plane change around the completion of one orbit.

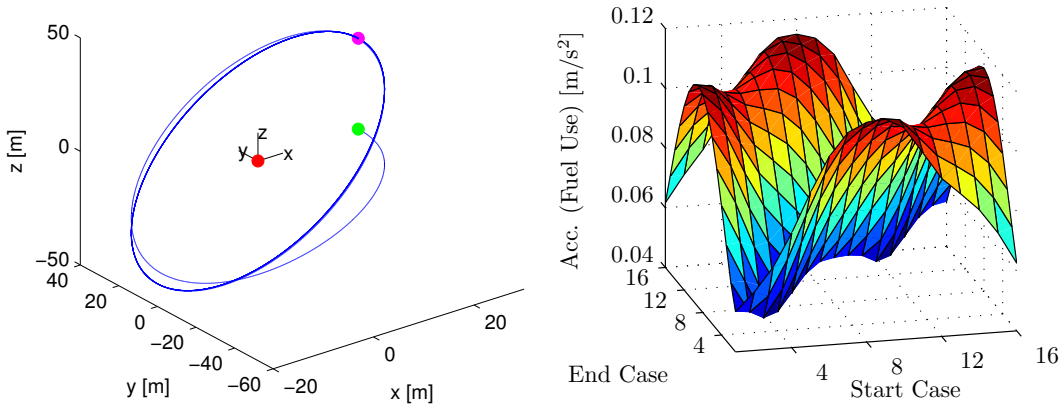

(a) Hill Frame Reconfiguration

(b) econfiguration acceleration budget

Figure 8. Reconfiguration between planar ellipse and circularly projected.

Consider the transfer shown in Figure 8(a) as one of many possible reconfigurations between the planar ellipse and a circularly projected orbit. Suppose that a family of reconfigurations between the planar and circularly projected are compared in acceleration requirement to distill possible optimal reconfigurations. Taking the condition shown in Figure 8(a) as the (1,1) case, Figure 8(b) sweeps a course grid of available transfers. The starting case number corresponds to a clockwise phased initial LROE set around the planar ellipse. The end case number corresponds to a clockwise phased end LROE set around the circularly projected orbit. Visible in Figure 8(b) is a substantial trough along

the diagonal. This corresponds to a matched initial and final phase of the LROE sets. As expected, maintaining the phase is the most fuel optimal approach. Further inspection demonstrates additional local minima along the matched phase trough. The two instances shown correspond to the ciruclarly projected orbit piercing the plane. Consistent with the classical Keplerian orbit elements, it is best to perform a plane change maneuver at the ascending and descending nodes, or plane crossings. The demonstration of this fuel optimality in the LROE set highlights the gemoterical intuition available and the opportunity for complete study into optimal transfers within LROE space. On-going work is expanding the optimality study throughout the entire LROE space to deliver broader optimal reconfiguration claims.

CONCLUSIONS

The modified LROE formulation derived from the classical CW equations and a feedback controller enables reconfiguration between relative orbits defined by LROE sets. The modified LROE formulation utilizes the Lagrangian Bracket evolution of invariant sets in the presence of accelerations to map relative orbit error into control accelarations. Three examples of the modified LROE controller is shown demonstrating a variety of available manuevers with around a circular chief. Also considered is the effect of perturbations to the LROE control implementation demonstrating that feed-forward may be possible. The patterned evolution of the relative orbit when using a modified LROE controller demonstrates the geometric insight of continuous acceleration relative orbit configuration.

In general, a new relative orbit feedback control law is developed and successfully tested in an inertial simulation. The control effort presented in the primary cases is under the thrusting magnitude of an ion thruster on approximately an 1000 kg spacecraft. Therefore the control magnitudes prescribed are feasible for continuous thrusting relative orbit reconfiguration. More simple relative configuration transfer planning may be possible through implementation of the presented LROE method. One limitation of the presented results is that the fundamental CW equations which give rise to the LROEs is a linear approximation of the motion. Therefore, the validity of the LROE approach is limited to maximum geometry dimensions less than a kilometer for negligible linearization error. Geometry greater than a kilometer begins to exceed the linearization assumptions used to develop the CW equations.

The interesting results presented suggest that both optimization and navigation using LROE sets are possible. Additional study will investigate more global fuel optimal claims when using LROE sets. Another potential variation of the presented control law is to develop an impulsive control strategy similar to the orbit element impulsive control strategy that is able to compute a series of impulse maneuvers to transition between relative orbits. This too would provide additional methods for creating relative motion reconfigurations. Use of LROE sets may also enable relative navigation schemes for rapid and/or course estimation of relative motion. There also exist alternate analytic forms of the CW equations that utilize a curvilinear representation to reduce the cartesian linearization error for geometries greater than 1 kilometer. The remaining challenge is characterizing disturbances and accelerations in curvilinear space. The presented study provides groundwork for future applications of the concepts described.

REFERENCES

[1] J. Schwartz and T. Krenzke, "Error-contracting impulse controller for satellite cluster flight formation," *AIAA Guidance, Navigation and Control Conference*, Boston, MA, August 19-22 2013.

[2] S. Chalt and D. A. Spencer, "PROX-1: Automated Trajectory Control for ON-Orbit Inspection," *37th Annual American Astronautical Society Guidance and Control Conference*, January 2014.

[3] H. Schaub, S. R. Vadali, and K. T. Alfriend, "Spacecraft Formation Flying Control Using Mean Orbit Elements," *Journal of the Astronautical Sciences*, Vol. 48, No. 1, 2000, pp. 69–87.

[4] H. Schaub and K. T. Alfriend, "Impulsive Feedback Control to Establish Specific Mean Orbit Elements of Spacecraft Formations," *AIAA Journal of Guidance, Control, and Dynamics*, Vol. 24, July–Aug. 2001, pp. 739–745.

[5] D. A. Vallado, "Orbital Mechanics Fundamentals," *Encyclopedia of Aerospace Engineering*, John Wiley & Sons, Dec. 2010, 10.1002/9780470686652.eae28.

[6] O. Montebruck, M. Kirschner, and S. D'Amico, "E/I-Vector separation for grace proximity operations," DLR/GSOC TN 04-08, 2004.

[7] E. Gill, S. D'Amico, and O. Montenbruck, "Autonomous Formation Flying for the PRISMA mission," *AIAA Journal of Spacecraft and Rockets*, Vol. 44, May–June 2007, pp. 671–681.

[8] C. Han and J. Yin, "Elliptical formation control based on relative orbit elements," *Acta Astronautica*, Vol. 77, Aug.-Sep. 2012.

[9] W. H. Clohessy and R. S. Wiltshire, "Terminal Guidance System for Satellite Rendezvous," *Journal of the Aerospace Sciences*, Vol. 27, Sept. 1960, pp. 653–658.

[10] T. A. Lovell and S. G. Tragesser, "Guidance for relative motion of Low Earth Orbit spacecraft base on relative orbit elements," *AIAA/AAS Astrodynamics Specialist Conference*, Providence, Rhode Island, August 16-19 2004.

[11] T. A. Lovell, S. G. Tragesser, and M. V. Tollefson, "A practical guidance methodology for relative motion of LEO spacecraft base on the Clohessy-Wiltshire equations," *14th AAS/AIAA Spaceflight Mechanics Meeting*, Maui, Hawaii, February 8–12 2004.

[12] R. Bevilacqua and T. A. Lovell, "Analytical guidance for spacecraft relative motion under constant thrust using relative orbit elements," *Acta Astronautica*, Vol. 102, 2014, pp. 47–61.

[13] A. C. Perez and T. A. Lovell, "Nonlinear representations of satellite relative motion equations using curvilinear transformations," *AAS*, 2015.

[14] T. A. Lovell and D. A. Spencer, "Relative Orbital Elements Formulation Based upon the Clohessy-Wiltshire Equations," *Journal of Astronautics*, February 2015.

[15] M. Humi and T. Carter, "The Clohessy-Wiltshire Equations can be Modified to Include Quadratic Drag," *Proceedings of the AAS/AIAA Spaceflight Mechanics Meeting*, Ponce, Puerto Rico, Feb. 9–13 2003. Paper No. AAS 03–240.

[16] C. R. Seubert and H. Schaub, "Tethered Coulomb Structures: Prospects and Challenges," *Journal of the Astronautical Sciences*, Vol. 57, Jan.–June 2009, pp. 347–368.

[17] H. Schaub and J. L. Junkins, *Analytical Mechanics of Space Systems*. Reston, VA: AIAA Education Series, 2nd ed., October 2009.

[18] D. A. Vallado, *Fundamentals of Astrodynamics and Applications*. Microcosm Press, 4th ed., March 2013.